# Journal of Materials Chemistry A

Accepted Manuscript


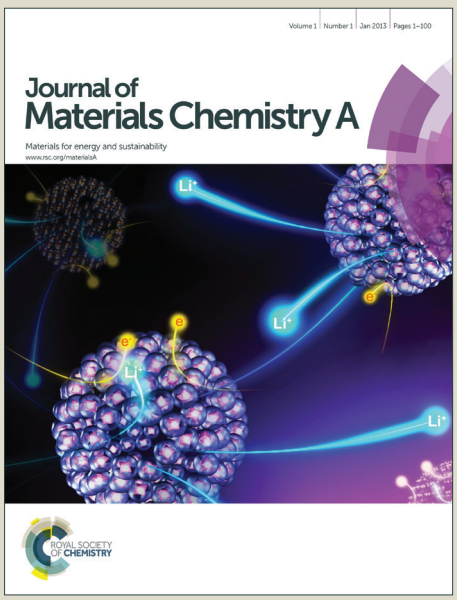





ROYAL SOCIETY OF CHEMISTRY

www.rsc.org/materialsA

Journal Name

RSCPublishing

ARTICLE

# Incorporation of Tin affects Crystallization, Morphology, and Crystal Composition of Sn-Beta

Cite this: DOI: 10.1039/xoxxoooooox

S. Tolborg,[a,b] A. Katerinopoulou,[b] D. D. Falcone,[c] I. Sádaba,[b] C. M. Osmundsen,[b] R. J. Davis,[c] E. Taarning,[b,*] P. Fristrup,[a] and M. S. Holm.[b]

Received ooth January 2012,
Accepted ooth January 2012

DOI: 10.1039/xoxxoooooox

www.rsc.org/

The crystallization of Sn-Beta in fluoride medium is greatly influenced by the amount and type of tin source present in the synthesis gel. By varying the amount of tin in the form of tin(IV) chloride pentahydrate, the time required for crystallization was studied. It was found that tin not only drastically affects the time required for crystallization, but also that the presence of tin changes the morphology of the formed Sn-Beta crystals. For low amounts of tin (Si/Sn = 400) crystallization occurs within four days and the Sn-Beta crystals are capped bipyramidal in shape, whereas for high amounts of tin (Si/Sn = 100) it takes about sixty days to reach full crystallinity and the resulting crystals are highly truncated, almost plate-like in shape. Using SEM-WDS to investigate the tin distribution along transverse sections of the Sn-Beta crystals, a gradient distribution of tin was found in all cases. It was observed that the tin density in the outer parts of the Sn-Beta crystals is roughly twice as high as in the tin depleted core of the crystals. Sn-Beta was found to obtain its maximum catalytic activity for the conversion of dihydroxyacetone to methyl lactate close to the minimum time required for obtaining full crystallinity. At excessive crystallization times, the catalytic activity decreased, presumably due to Ostwald ripening.

## Introduction

Sn-Beta is a zeotype material containing tin incorporated in the zeolite framework. The crystalline material has strong Lewis acidic properties, attributable to discrete tin sites, as well as a microporous network characteristic of a zeolite system. These two features combined with sufficiently large pores have made this material a promising catalyst for a range of industrially relevant reactions. Sn-Beta has been shown to be an active catalyst for Meerwein-Ponndorf-Verley-Oppenauer redox reactions as well as for Baeyer-Villiger oxidations where the use of hydrogen peroxide with Sn-Beta makes it possible to avoid the use of expensive peracids.[1, 2] In recent years other interesting potential uses of Sn-Beta have been explored within the emerging area of biomass conversion.[3, 4] The catalytic synthesis of lactates from sugars is one such example where Sn-Beta has been found to be a useful catalyst.[3, 5-7] The production of this biodegradable plastic monomer is otherwise restricted to base catalyzed conversion of sugars and fermentation.[8-10] Apart from this reaction, Sn-Beta also catalyzes the isomerization of monosaccharides e.g. glucose to fructose.[4, 6, 11]

Fundamental studies have revealed the presence of two or more configurations of the framework tin site.[11-13] This was achieved using a combination of computational studies with advanced techniques such as cross polarization nuclear magnetic resonance, infrared spectroscopy, and thermogravimetric measurements using a variety of probe molecules.[11-16]

In spite of the interest in Sn-Beta, fundamental aspects of the effect of tin during the preparation of the catalyst are still not fully understood. It is well-known from preparation of other zeolite structures that even small variations in the composition of the gel during synthesis can have great impact on the resulting material. For instance, changing pH, silica-source, structure directing agent (SDA), water content, and the use of agitation during the synthesis have all been shown to affect the crystallization behavior for other zeolites.[17-21]

The traditional procedure for synthesizing Sn-Beta involves fluoride media at near neutral pH as described by Corma,[1, 3, 11, 22] but it has also been prepared in hydroxide media.[22] The role of the mineralizing agent is to dissolve and transport silica species during the formation of the zeolite framework.[23] Due to the strong interaction between the fluor and the silica-species, fluoride ions can advantageously be used as the mineralizing agent.[1, 24, 25] The fluoride route produces largely defect-free and hydrophobic materials as well as larger crystals, in the order of several µm, compared to the hydroxide counterparts where crystals of only a few hundred nanometers in diameter are obtained. This can be explained by the low degree of supersaturation obtained with fluoride ions as the mineralizing agent, which effectively limit nucleation in the preliminary steps of zeolite formation.[26] This also affects the crystallization

time of the materials, as the time required to obtain a fully crystalline zeolite increases drastically. Seeding is therefore often used to accelerate the crystal growth to overcome this.[27, 28] Although a reduction of the crystallization time is observed, the induced nucleation severely affects the crystal morphology of the sample, typically resulting in intergrown zeolite crystals forming larger agglomerates, which cannot be distinguished in a micrograph.[14]

Studies have shown that it is possible to reduce the crystallization time and crystallite sizes either by extensive seeding, steam-assisted conversion or through post-synthetic methods.[29-32] The aim of this fundamental study is to identify the effect of the presence of tin on the synthesis of Sn-Beta materials on the crystal morphology, crystallization time and distribution of tin in the individual crystals. The original fluoride-route synthesis described by Valencia *et al* is therefore used to obtain the larger crystals that can then be analyzed by advanced spectroscopic techniques in the electron microscope.[33]

In previous reports, the tin content is generally kept low with Si/Sn ≥ 100, since it has been noted that tin retards the crystal formation.[1, 3, 4] However, a more systematic analysis of the processes involved in the synthesis is required to fundamentally understand the effect of the tin in the preparation of the Sn-Beta materials. Understanding the role of tin could help increase the amount of active sites which can be incorporated in the zeolite framework. The exact distribution of tin in the crystal is not known, and it will also be addressed in this study.

Several of the reactions that Sn-Beta is known to catalyze are liquid phase reactions where diffusion limitations are expected to be an even more important factor than in gas phase reactions. The understanding and control of the crystal morphology as well as the accessibility to the active tin sites are therefore important for the activity of the catalyst.

We show here that the incorporation of tin not only introduces Lewis acid sites in the zeolite material but also directly affects the growth kinetics and the morphology of the resulting crystals. Additionally, we show by ways of wavelength dispersive spectrometry (WDS) of transverse cuts of Sn-Beta crystals that tin is not evenly distributed in the bulk crystal but rather localized as a tin-rich shell.

## Experimental

### 2.1. Synthesis

The reagents used for the synthesis of Si-Beta and Sn-Beta were tetraethylammonium hydroxide (TEAOH, Sigma-Aldrich, 35% in water), tetraethylorthosilicate (TEOS, Aldrich, 98%), hydrofluoric acid (HF, Fluka, 47-51%), tin(IV) chloride pentahydrate ($SnCl_4 \cdot 5H_2O$, Aldrich, 98%), tin(IV) oxide ($SnO_2$, Aldrich, <100 nm particle size), tin(IV) acetate ($Sn(CH_3CO_2)_4$, Aldrich), and ammonium hexafluorostannate ($(NH_4)_2SnF_6$, Aldrich, 99.999%). All reactants were used without further purification.

The Sn-Beta zeolites were synthesized by modifying the route described by Valencia *et al*.[33] Since seeding makes any investigation of morphology difficult, the synthesis procedure used in this study does not involve the use of seeds in the preparation of the materials. In a typical synthesis procedure, 30.6 g of TEOS was added to 33.1 g of TEAOH under careful stirring, forming a two-phase system. After 60-90 min, one phase was obtained and the desired amount of the tin source, typically $SnCl_4 \cdot H_2O$, dissolved in 2.0 mL of $H_2O$ was added drop-wise. The solution was then left for several hours under stirring until a viscous gel was formed. The gel was finalized by the addition of 3.1 g HF in 1.6 g of demineralized $H_2O$ yielding a solid gel with the molar composition; $1.0Si{:}xSn{:}4xCl^-{:}0.55TEA^+{:}0.55F^-{:}7.5H_2O$, where $x$ ranged from 0.0025 to 0.01. Purely siliceous Beta was prepared following the same route only leaving out the addition of the tin source. All samples were then homogenized and transferred to a Teflon-lined stainless steel autoclave and heated statically at 140°C for a duration ranging from 2 to 60 days to obtain samples covering a wide range of crystallinities. The obtained solid was recovered by filtration and washed with ample amounts of deionized water, followed by drying overnight at 80°C in air. The synthesis was finalized by removing the organic template by heating the sample at 2°C/min to 550°C in static air and maintaining this temperature for 6 hours.

Tetraethylammonium hexafluorostannate, $(TEA)_2SnF_6$, as an alternative tin source, was adapted from procedures reported previously.[26] Prior to the synthesis, the desired amount of $(NH_4)_2SnF_6$ was added to the 33.1 g of TEAOH (35%) used for a typical synthesis. The mixture was then placed under rotation at 0.2 bar for 20 min at room temperature to allow ammonia to evaporate and the tin source to form. This $(TEA)_2SnF_6$/TEAOH mixture was then used as the tin source and SDA with no additional tin added to the system.

### 2.2 Characterization

Powder X-ray diffraction (XRD) patterns of the calcined samples were measured on an X'Pert diffractometer (Philips) using Cu-Kα radiation. Crystallinities (in %) of the prepared samples were calculated using the TOPAS software following the PONCKS method described by Scarlett and Madsen.[34]

The elemental composition of the prepared materials was measured using inductively coupled plasma atomic emission spectroscopy (ICP-OES). The zeolite samples were fully dissolved in a mixture of HF, HCl, $HNO_3$ $H_3PO_4$, followed by neutralization of excess HF by the addition of $B(OH)_3$, and then measured on the Perkin Elmer model Optima 3000 (Varian Vista).



 

Table 1. Physical properties of samples with nominal Si/Sn ratio of 200.

| Entry | Crystallization | Crystallinity[a] | Tin[b] | Si/Sn[b] | $S_{BET}$[c] | $V_{micropore}$[d] |
|---|---|---|---|---|---|---|
| | days | % | wt % | | $m^2/g$ | mL/g |
| 1 | 2 | 8 | 0.93 | 211 | 395 | 0.10 |
| 2 | 4 | 52 | 0.90 | 219 | 422 | 0.14 |
| 3 | 5 | 60 | 0.91 | 217 | 437 | 0.16 |
| 4 | 7 | >95 | 0.97 | 203 | 471 | 0.19 |
| 5 | 14 | >95 | 0.96 | 204 | 473 | 0.19 |
| 6 | 30 | >95 | 0.94 | 209 | 475 | 0.20 |

a. Determined by Rietveld refinement of XRD measurements using the PONCKS method.
b. Determined by ICP analysis.
c. BET surface area
d. Micropore volume, calculated using the *t*-plot method.

Surface area and pore volume measurements were per-formed using multipoint $N_2$ adsorption/desorption on an Autosorb automatic surface area and pore size analyzer (Quantachrome Instruments). The total surface area of the samples was obtained using the BET method and the micropore volume was calculated by the t-plot method using the Autosorb3 software.
Secondary electron (SE) and backscattered electron (BSE) images of the investigated samples were obtained on a XL30 field emission scanning electron microscope (FEI) operated at 5 kV. To ensure uniform electrical properties and to avoid charging effects samples were coated with Pt/Pd or Au
Element maps were measured with a JXA-8530F field emission electron probe micro analyzer (JEOL) operated at 10 kV and 7 nA. Crystals were mounted in epoxy and polished to expose cross sections through the grains. The surface of the mounts was coated with carbon prior to analysis. Maps were collected by beam rastering over the crystal area. Due to material instability under the beam, maps were collected with low dwell times and several accumulations. Beam tracking was applied to avoid lateral drift, which would affect the spatial resolution.
Characteristic X-Rays were analyzed on a TAP crystal (Si) and PETH crystal (Sn). In order to avoid geometrical effects that could introduce errors on the analysis, Sn was measured on two spectrometers situated at 90° to each other. Maps acquired with these spectrometers were identical.

### 2.3 Catalytic testing

Catalytic conversion of 1,3-dihydroxyacetone (DHA) in methanol to methyl lactate (ML) was performed under autogenous pressure in 10 mL thick-walled glass reactors (ACE) placed in a preheated oil bath at 75°C. Typically, 300 mg (3.33 mmol) of DHA, 25 mg of catalyst, and 6.5 mL of methanol were added to the ACE-vial. The vessel was then heated and vigorously stirred for 2 hours, followed by quenching in cold water. After the reaction, the reaction liquid was analyzed using a 7890A Series GC system (Agilent Technologies) with a SolGel-WAX column (Phenomenex) to quantify the ML yield.

Leaching experiments were carried as follows. Catalyst Sn-Beta zeolite (25 mg) was treated in 6.5 mL of methanol at 75 °C for 2 hours. After this time, the catalyst was filtered off and this methanol was used as the solvent for the reaction under the previous conditions.

## Results and discussion

### 3.1 Effect of tin on crystallization time

The effect of tin in the gel on the crystal growth of Sn-Beta was studied in a series of fluoride syntheses conducted at near neutral pH. A matrix of Sn-Beta samples was prepared with all synthesis parameters kept unchanged except the amount of tin in the form of $SnCl_4 \cdot H_2O$ added to the system and the crystallization time. Different nominal Si/Sn rations were prepared (100, 150, 200, 400) using different crystallization times for each tin content (2, 4, 5, 7, 14, 30, 45 and 60 days).The temperature during crystallization was kept constant at 140°C. Higher temperatures were found early on to favor the formation of the MFI zeolite framework.

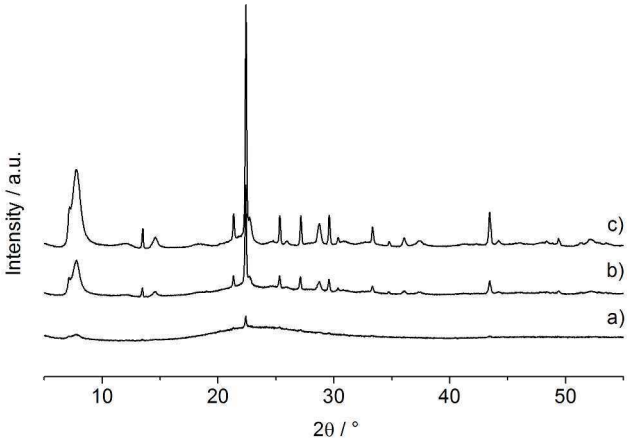


Figure 1. X-ray diffraction patterns of Sn-Beta samples with Si/Sn = 200 crystallized for a) 2, b) 4, and c) 7 days. The latter is representative of an X-ray diffraction pattern of a fully crystalline Sn-Beta material.

Table 1 summarizes the crystallinity, tin content, crystal size and pore system measurements for samples synthesized with 1 wt% tin (Si/Sn = 200) in the gel. Physical properties for the remaining samples can be found in Table S1.

The relative crystallinity of the prepared samples was followed using XRD. Figure 1 shows the XRD diffractograms of samples synthesized with ~1.0% tin in the gel with the synthesis being terminated after 2, 4 and 7 days, respectively. A gradual change in crystallinity is clearly observed as the sample is almost entirely amorphous (8% crystallinity, Table 1, entry 1) after 2 days (Figure 1a) increasing to 52 % crystallinity (Table 1, entry 2) after 4 days. After 7 days, a well-crystallized Sn-Beta sample is obtained (>95% crystallinity, Table 1, entry 4) with only trace amounts of the amorphous background (Figure 1c). SE images of these samples can be seen in Figure S1. Once fully crystallized, no changes in the XRD diffractograms are observed for samples left at synthesis temperature for excessive duration, *e.g.* 14 and 30 days. The relative crystallinity of these samples likewise remained at >95% (Table 1, entries 4-6). In all the cases, no other phases were observed, except the *BEA framework of the Beta zeolite. Even at very long crystallization times and with large quantities of tin in the synthesis mixture, no formation of MFI framework structure was detected. MFI is often found as a secondary phase when varying the synthesis conditions of Beta zeolites.[26]

Table 2. Physical properties of Sn-Beta samples with varying tin content after obtaining full crystallinity (> 95 %).

| Entry | Si/Sn[a] | Crystallization | Tin[b] | $S_{BET}$[c] | $V_{micropore}$[d] |
|---|---|---|---|---|---|
| | | days | wt% | $m^2/g$ | mL |
| 1 | - | 4 | - | 459 | 0.19 |
| 2 | 400 | 4 | 0.42 | 464 | 0.19 |
| 3 | 200 | 7 | 1.00 | 471 | 0.19 |
| 4 | 150 | 14 | 1.24 | 470 | 0.20 |
| 5 | 100 | 60 | 1.81 | 508 | 0.20 |

a. Nominal.
b. Determined by elemental analysis (ICP).
c. BET surface area.
d. Calculated using the t-plot method.

Independent of the degree of crystallinity, the tin content in the washed and calcined material is found to vary little (0.90-0.97 wt%) in the series as detected by ICP-OES, see Table 1. These values correspond to 92-96% of the tin present during synthesis, and thus close to all tin is recovered in the finished solid. However, in almost all samples, small tin oxide nanoparticles were found on the surface of the formed crystals by investigating the sample series using the back-scatter detector in SEM, see Figure S2. The tin content in the samples is determined by dissolution of the zeolite material and quantification by ICP-OES. Therefore, nanoparticles of tin oxide will be detected along with tin incorporated into the framework. Importantly, this means that not all tin added to the synthesis gel is actually incorporated into the framework forming active sites. At present it is unclear whether the tin oxide is formed during the hydrothermal synthesis or during cooling of the gel after the synthesis has finished, where tin species could precipitate on the crystals and be converted into tin oxide during calcination A quantitative determination of the amount of tin in the form of tin oxide still remains a challenge in this material.

The surface area and pore volume of the prepared samples undergo a similar development during crystallization. By using $N_2$ adsorption/desorption, the surface area ($S_{BET}$) and micropore volume ($V_{micropore}$) could be followed. A typical Sn-Beta zeolite (Si/Sn = 200) has a $S_{BET}$ and $V_{micropore}$ of 450-500 $m^2/g$ and 0.20 mL/g, respectively.[14] The total surface area increases from 395 to 471 $m^2/g$ (Table 1, entries 1-4) with the increase in crystallinity from 8% to >95% (from 2 to 7 day crystallization), remaining at ~475 $m^2/g$ for longer crystallization times (Table 1, entries 4-6). For the micropore volume a similar trend is observed, increasing from 0.10 to 0.19 mL/g at the point of crystallization and remaining at ~0.20 mL/g beyond this point (Table 1, entries 1-6). The crystallinities determined by Rietveld refinement are thus corroborated by surface area and pore volume measurements.

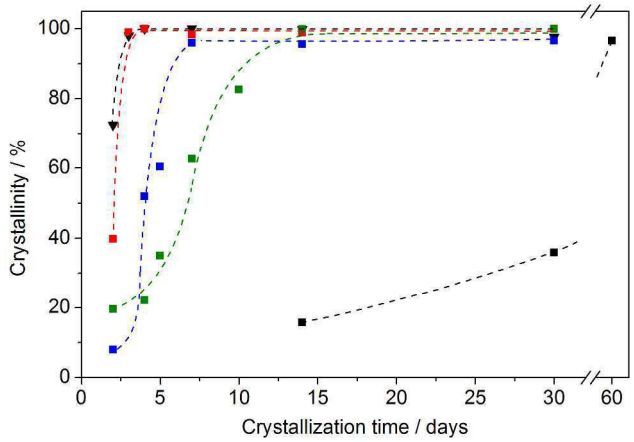


Figure 2. Crystallinity of Sn-Beta samples of varying hydrothermal synthesis times and with Si/Sn ratios of 100 (▪), 150 (▪), 200 (▪), 400 (▪) and without tin (▼). The lines are a guide to the eye.

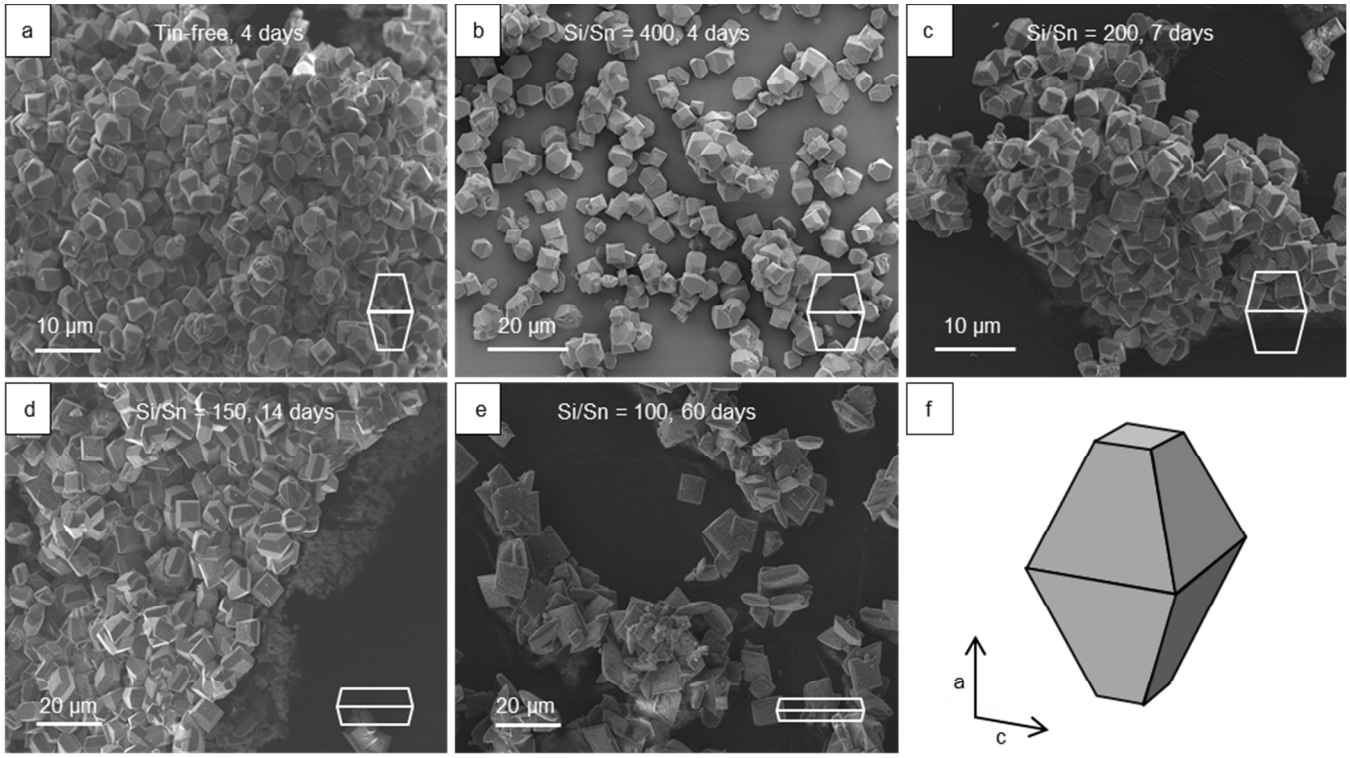


Figure 3. SEM imaging of Sn-Beta crystals synthesized with a Si/Sn ratio and crystallization time of a) tin-free, 4 days, b) 400, 4 days c) 200, 7 days d) 150, 14 days and e) 100, 60 days. On f) the capped bipyramidal morphology of Sn-Beta is shown with the a and c direction presented.

For samples with varying tin contents, the crystallinity values obtained from XRD results were plotted as a function of the crystallization time, see Figure 2 (SE images of these samples can be found in SI). The hydrothermal synthesis time required to obtain Sn-Beta samples of high crystallinity (>95%) was found to vary greatly with the amount of tin present in the synthesis mixture. When no or low amounts of tin (0.5 wt% for Si/Sn = 400) were present during the synthesis, fully crystalline Beta samples could be obtained after only 4 days. Increasing the tin content to 1.0 wt% (Si/Sn = 200) increased the required time to 7 days and further tin addition increased the required synthesis time to 14 days for 1.3 wt% (Si/Sn = 150) and up towards 60 days for 1.9 wt% (Si/Sn = 100). Table 2 shows the structural and material properties of the fully crystalline samples for every tin content series. Even at very long crystallization times, very little difference in the material and structural properties of the zeolites are observed with only a slightly higher surface area for samples of very high tin content (Table 2, entry 5).

The retardation in the synthesis caused by tin clearly shows the impracticality of preparing Sn-Beta catalysts with higher tin loadings (Si/Sn < 100). This practically limits the amount of active tin sites that can be present in a catalyst synthesized in a fluoride medium.

### 3.2 Effect of tin on morphology and crystal composition

To study the impact of tin on the crystal growth and morphology of the individual Sn-Beta crystals, analysis by electron microscopy was applied. All crystalline samples in the sample series had the capped square bipyramidal (CSBP) morphology typical to the Beta zeolite system, see Figure 3f.[35] The elongated CSBP crystal morphology of the purely siliceous Beta (Figure 3a) resemble what is found in literature in comparable synthesis systems.[36]

Table 3. Changes in the crystal size and aspect ratio (*a*/*b*) of the formed crystals as investigated by SEM. The crystal size is listed as an average of a minimum of 10 crystals.

| Entry | Si/Sn | Crystallization Days | Crystal size µm | *a*/*b* |
|---|---|---|---|---|
| 1 | - | 4 | 3.4 ± 0.7 | 2.3 |
| 2 | 400 | 4 | 5 ± 1 | 1.7 |
| 3 | 200 | 7 | 4.0 ± 0.7 | 1.6 |
| 4 | 200 | 14 | 7 ± 1 | 1.5 |
| 5 | 200 | 30 | 11.8 ± 0.9 | 1.5 |
| 6 | 150 | 14 | 7 ± 1 | 1.4 |
| 7 | 100 | 60 | 8 ± 3 | 1.1 |

a. Crystal size measured from SEM as the length across the pyramidal base (a).

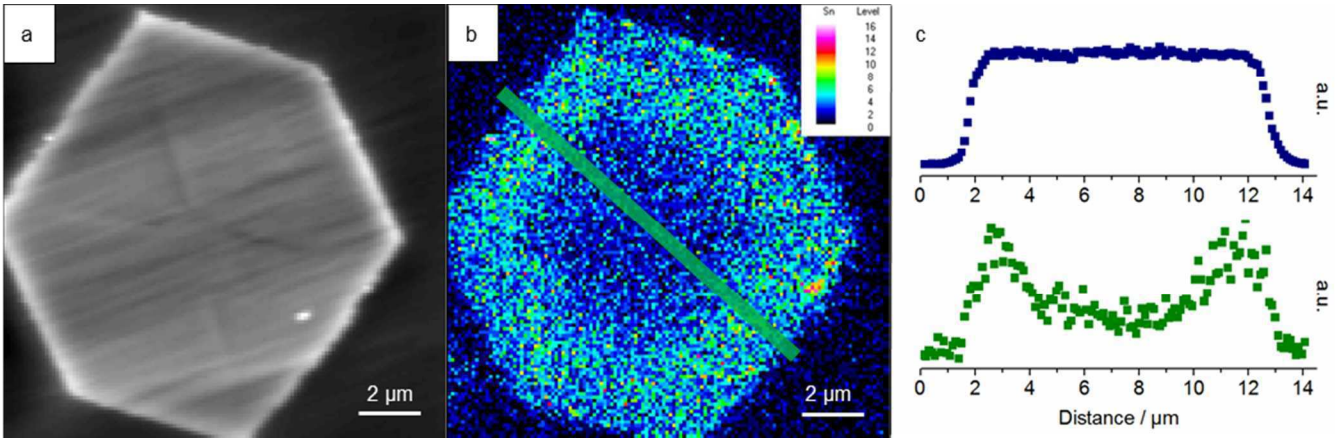


Figure 4. WDS analysis of a Sn-Beta sample (Si/Sn = 200) crystallized for 30 days showing a) SE image of the investigated crystal, b) Sn X-Ray intensity, and c) X-ray intensities for Si (▪) and Sn (▪). The data for c) were extracted from the map at the area indicated by the green outline on b) and averaged across the thickness of the line.

Interestingly, the addition of tin has a clear effect on the morphology. When tin content increases (Si/Sn ratios = 200, 150 and 100), a systematic change in the morphology of the resulting Sn-Beta crystals was observed, see Figure 3. The growth of the pyramidal (*h0l*) face is significantly decreased (c direction on Figure 3f), while the pinacoidal (*00l*) face is increased (a direction on Figure 3f). This is observed as a considerable decrease in the height of the crystal, while the squared base of the pyramidal morphology is expanded (Figure 3a-e). At very high tin content (Si/Sn = 100 crystallized for 60 days), the result is an almost plate-like CSBP morphology.

The length of the pyramidal (*a*) and plateau (*b*) edges has previously been used to track the changes in the morphology of capped bipyramidal crystals.[35] Measuring distances on images obtained from SEM can be difficult and requires the precise knowledge of the geometry between the orientation of the crystal and the detector. With no reference this makes measuring a height of the crystals inaccurate at best. The two lengths *a* and *b* are individually complicated to measure precisely, but given the parallelism of the two edges and thus the equal orientation relative to the detector, the ratio *a*/*b* of the individually measured crystals can be determined far more precisely, see Figure S3. In Table 3 the average crystal size and the ratio *a*/*b* of the zeotype crystals are given. Samples were measured once full crystallinity (>95%) was reached.

From purely siliceous Beta (Table 3, entry 1) to samples with a Si/Sn ratio of 100 (Table 3, entry 7), a decrease in the *a*/*b* ratio from 2.3 to 1.1 is observed, suggesting a direct correlation between the tin content and the degree of the morphological changes (Figure 5). The growth rates of the individual crystal faces determine the overall crystal morphology. Faces with a high growth rate become more pronounced in the final morphology compared to faces with slow growth.[26] This suggests that the addition of tin to the synthesis mixture changes the growth of the pyramidal and pinacoidal faces, making the plateau of the crystal the dominant feature with higher tin loadings. This morphology transformation could have an effect on the resulting catalytic ability of the material as the preferred representation of the channel system is significantly altered, however any changes caused by this effect were not possible to disentangle from simultaneous increase in tin content.

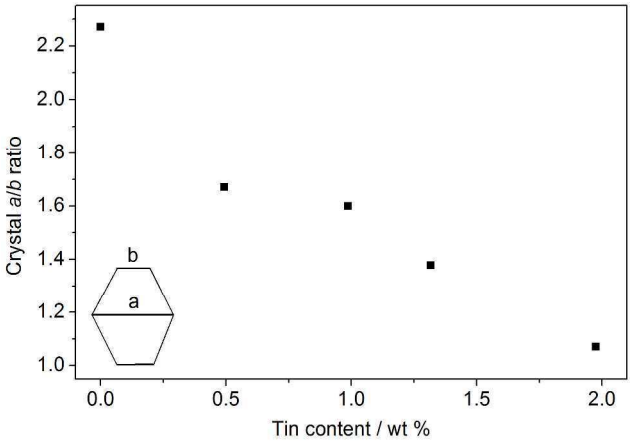


Figure 5. The *a*/*b* aspect ratio measured for samples of varying tin content after full crystallization (>95 % crystallinity).

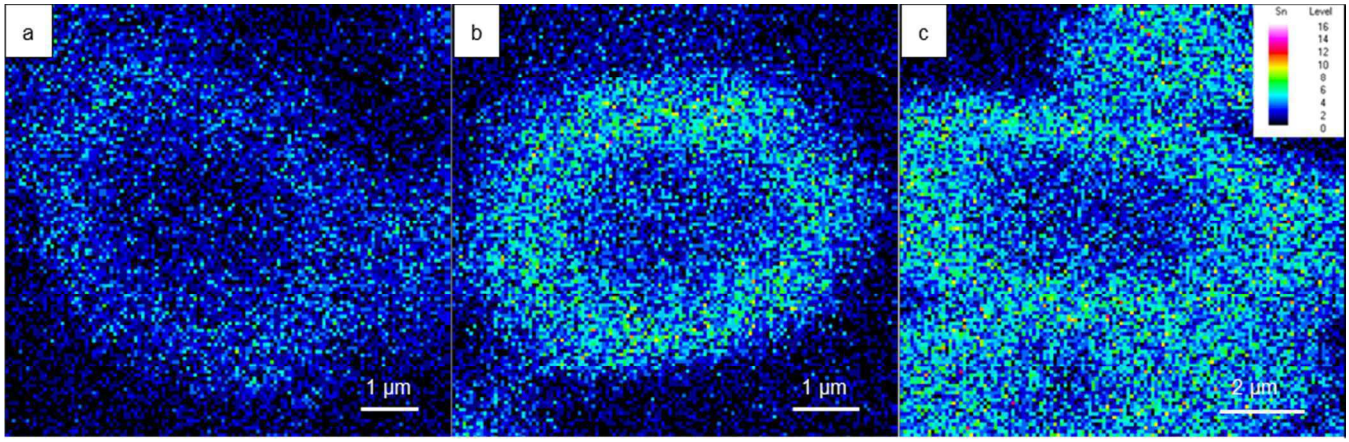


Figure 6. SEM-WDS measurements showing the tin distribution in transverse sections of Sn-Beta zeolites with Si/Sn ratios of a) 400 (crystallized for 4 days), b) 200 (7 days) and c) 100 (60 days).

It is important to note that although no change is observed for the physical properties of the zeolite samples after full crystallinity is reached (Table 1, entries 4-6), crystals are known to undergo Ostwald ripening.[37, 38] This process consist of the dissolution and redepositing of smaller crystals onto larger ones and results in an overall continued growth of the average crystal size of the sample even after a fully crystalline material has been obtained.[37, 38] In Table 3 entries 3-5, the Ostwald ripening effect is shown for the Si/Sn = 200 sample series. Upon full crystallization after 7 days, an average base length (a) of 4.0±0.7 µm was measured (Table 3, entry 3) which increased to 7±1 µm (Table 3, entry 4) and 11.8±0.9 µm (Table 3, entry 5) after 14 and 30 days, respectively. This restructuring could have an impact on the catalytic activity of the material, not only due to diffusion limitations introduced with larger crystals but also caused by changes in the environment of tin. A potential consequence of the ripening process could be an increased formation of inactive tin oxide species, although this was not confirmed in this study. The aspect ratio *a*/*b* was found to remain constant for Si/Sn = 200 at ~1.6 (Table 3, entries 3-5), showing that although crystal growth continues with longer synthesis time, ripening does not affect the morphology. The morphology is thus dictated by the tin content and not the time of crystallization.

The morphology of the samples is very important with respect to catalyst activity but the distribution of tin in the framework could have an even greater importance. To investigate the incorporation of tin in the crystals, transverse cuts of the samples of various tin contents and synthesis times (Table 2) were prepared and investigated by SEM with a wavelength-dispersive spectrometer (WDS). For a number of transverse cuts of the array of Sn-Beta crystals, lines protruding from the center towards the corners were observed, see Figure 4. This is known as the '*hourglass phenomenon*' and is believed to be caused by the continuous incorporation of defects during the crystal growth, where the crystal faces meet.[39, 40]

Using SEM-WDS, it was possible to select and accurately map the elemental composition of crystal transections. In all the cases where the CSBP morphology was clearly visible as a symmetrical hexagonal geometry (Figure 5a), a clear gradient was observed in the distribution of tin in the zeolite crystal, see Figure 5b. In Figure 5c, the X-Ray intensity from Si and Sn was measured across a Sn-Beta crystal from a sample crystallized for 30 days with a Si/Sn ratio of 200. The measurement for silicon shows a constant level throughout the crystal, but a clear decrease in tin content can be seen towards the center of the crystal (Figure 5c). After acquisition of the maps, the signal on each pixel was processed. A fixed background was substructed and full ZAF standard-based correction routine was applied to produce quantitative results. Due to the large difference between the acquisition time of calibration intensities and the dwell time of mapping, the quantitative results can only show a relative difference in concentrations rather than absolute mass concentrations. Applying this technique to the measurement shown in Figure 5b, it was found that the rim contained approximately twice as much tin compared to the center.

The enriched outer shell of tin was observed for all tin-containing samples irrespective of the resulting morphology changes and the size of the formed crystals. Figure 6 shows the tin distribution in Sn-Beta crystals with Si/Sn ratios of 400, 200, and 100, respectively (additional examples can be found in SI). All show the same decrease in tin concentration towards the center of the zeolite crystal with a thickness of the shell varying from 1-2 µm. This shows that tin is primarily found as a shell with a thickness corresponding to roughly half the distance along the center of the crystal independent of the amount of tin incorporated in the material. The tin distribution was also found in transection before and after calcination showing that it is not caused by a thermal redistribution (see Figure S4). This gradient in the tin distribution within the bulk crystal has to our knowledge not previously been observed for this material.

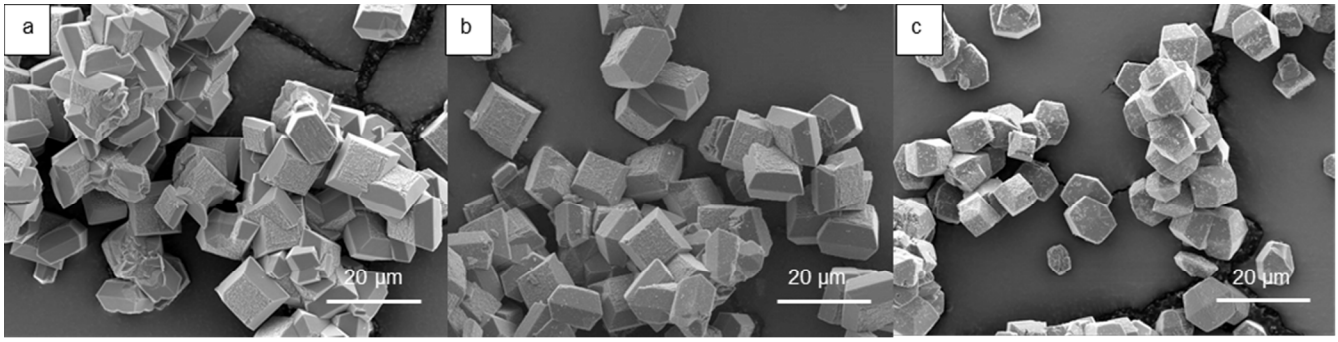


Figure 7. SEM images of Sn-Beta samples crystallized for 14 days using a) tin(IV) acetate, b) $(TEA)_2SnF_6$ and c) $SnO_2$ (<100 nm) as the tin source.

Since a continued growth of the zeolite crystals was observed with longer synthesis times, presumably due to Ostwald ripening effects, it was important to investigate the evolution of this outer layer of tin within the crystal over time. Samples of different crystallization times from 4 to 30 days and Si/Sn = 200 (Table 2, entries 3-6) were investigated. Throughout this sample series, a clear difference in average crystal size was measured ranging from 4.0 to 11.8 µm. It was discovered that the tin layer likewise changes in thickness. Differences in the shell thickness of samples crystallized for 2-14 days were not large enough to indicate any significant difference and the thickness of these samples were all in the 1-2 µm range, generally corresponding to ~50% of the crystal radius. For the very large crystals obtained after 30 days (Figure 5) with a pyramidal length of 11.8 µm, however, the measured thickness of the tin layer was consistently 3-3.5 µm. Although the tin shell is much larger for this crystal, it is still found to correspond to ~50% of the radial distance, meaning that the internal void with low tin concentration likewise must have grown in size. This is corroborated by the fact that the tin shell was found in all samples, including those with poor crystallinity containing only the semi-crystalline monomer crystal shapes. This is surprising as one would expect growth from nucleation to crystal to occur radially, where a difference in tin concentration would then be caused by a late incorporation of tin during the synthesis. The fact that tin is already incorporated in what later becomes the catalyst crystals at such early stages, hints that tin is incorporated as part of the '*solid-phase transformation process*', where the T-O-T bonds within the solid are continuously formed and broken initially to form the crystalline solid from the amorphous phase and later to mediate the further growth brought on by Ostwald ripening between crystals.[41]

Some authors have proposed that the changes in morphology during zeolite synthesis are due to variations in the pH of the synthesis gel.[42] In order to investigate whether the tin salt is responsible for the resulting change in crystals morphology, Sn-Beta samples with a Si/Sn ratio of 150 were prepared using different tin sources and crystallized for 14 days. Tin(IV) oxide nanoparticles ($SnO_2$, <100 nm), tin(IV) acetate ($Sn(CH_3CO_2)_4$) and tetraethylammonium hexafluorostannate ($(TEA)_2SnF_6$) were used as the source of tin. All other synthesis parameters were kept constant. Tin(IV) oxide is insoluble in the synthesis gel, tin(IV) acetate eliminates the presence of chloride ions and the use of tetraethylammonium hexafluorostannate allows the synthesis without introducing any external anion in the synthesis gel. Physical properties for these samples can be found in Table S2.

Table 4. Sn-Beta samples (Si/Sn = 150) prepared with different tin sources synthesized at hydrothermal conditions for 14 days.

| Entry | Tin source | Crystal size[a] µm | | | *a*/*b* |
|---|---|---|---|---|---|
| 1 | $SnCl_4{\cdot}5H_2O$ | 7 | ± | 1 | 1.4 |
| 2 | $Sn(CH_3CO_2)_4$ | 8 | ± | 2 | 1.3 |
| 3 | $(TEA)_2SnF_6$[b] | 10 | ± | 2 | 1.4 |
| 4 | $SnO_2$[c] | 6.6 | ± | 0.9 | 1.6 |

a. Crystal size measured from SEM as the length across the pyramidal base (*a*).
b. $(NH_4)_2SnF_6$ added to TEAOH, $NH_3$ removed by evaporation at 0.20 bar under stirring.
c. $SnO_2$ particles < 100 nm.

Both tin(IV) acetate and $(TEA)_2SnF_6$ yielded highly crystalline, truncated crystals with very similar *a*/*b* ratios (*a*/*b* = 1.3-1.4, Table 4, entries 2-3) as samples prepared using tin(IV) chloride (*a*/*b* = 1.4, Table 4, entry 1). The morphology of these two Sn-Beta samples (Figure 7a and b) is comparable to what was found for the standard conditions using tin(IV) chloride (Figure 3d). When $SnO_2$ nanoparticles were used as tin source, the resulting crystals were more elongated in shape (Figure 7c), making the *a*/*b* ratio higher (*a*/*b* = 1.6, Table 4, entry 4), thus more comparable to purely siliceous Beta samples (Figure 3a).

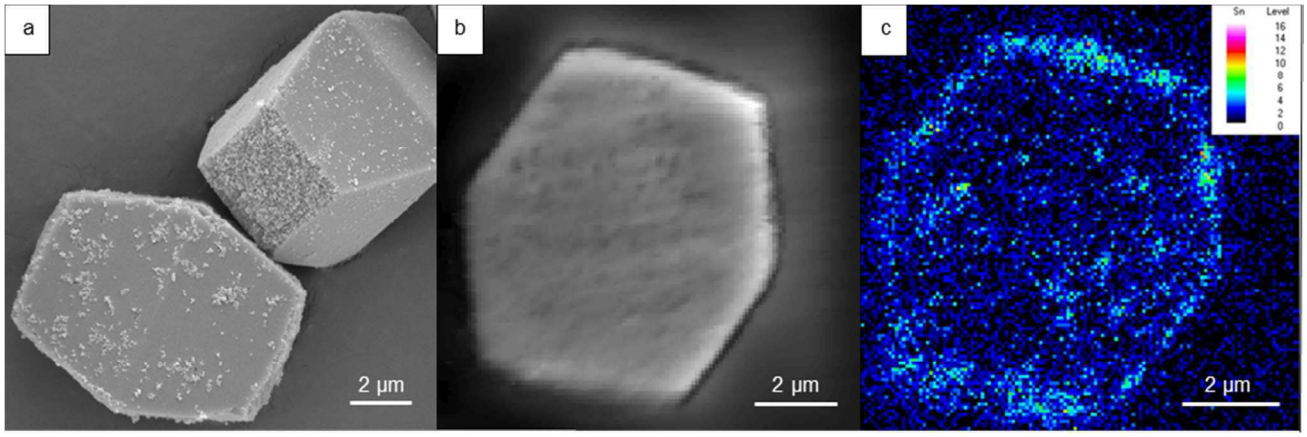


Figure 8. a) SEM image of Sn-Beta crystals prepared using $SnO_2$ as tin source, b) SE image of the transected $SnO_2$-Sn-Beta crystal and c) the X-ray intensities of tin of b).

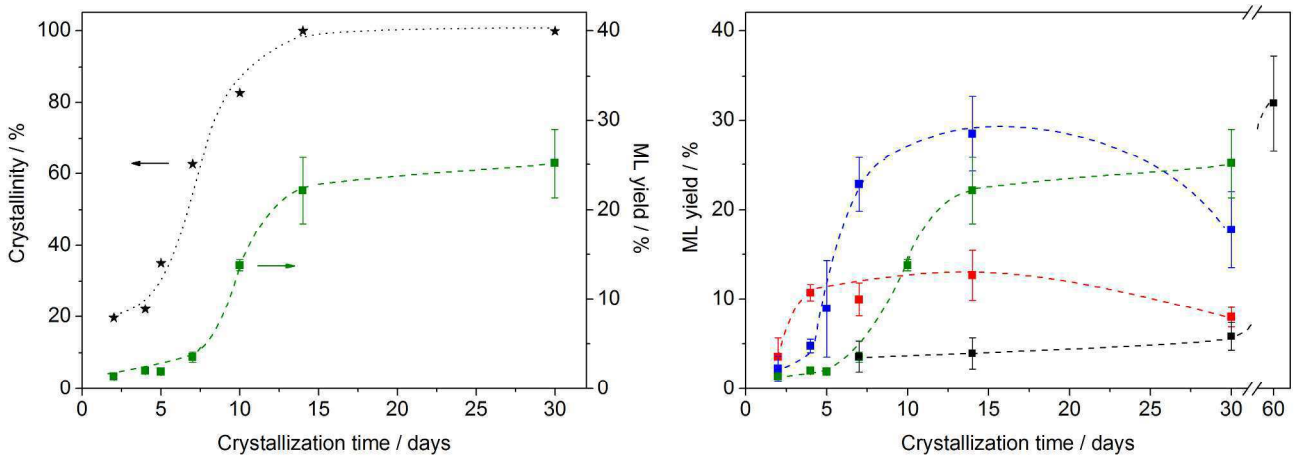


Figure 9. a) Crystallinity (★) and methyl lactate yield (▪) obtained with Sn-Beta samples (Si/Sn = 150) prepared at varying hydrothermal synthesis times. b) Yield of ML obtained using Sn-Beta samples crystallized for a varying amount of days and with a Si/Sn ratio of 100 (▪), 150 (▪), 200 (▪) and 400 (▪). Reaction conditions: 25 mg catalyst, 300 mg DHA, 6.5 mL methanol, 600 rpm, 75°C, 2 hours. Each experiment was performed a minimum of 3 times. The lines are a guide to the eye.

We believe that no tin is incorporated in the zeolite framework in this sample due to the insolubility of the tin source. From the elemental map very little tin is found to be contained within the crystal (Figure 8c). Instead highly localized tin concentrations were found on the edges of the crystals, see Figure 8a and Figure 8c. The surface of the crystals from this sample was covered with small particles found to be $SnO_2$. As a result, when tin is not incorporated in the framework, no enriched tin shell or change in morphology are observed.

Sn-Beta samples where tin was successfully incorporated in the framework using alternative tin sources such as tin(IV) acetate or $(TEA)_2SnF_6$ were found to give rise to a similar tin gradient. Therefore, it can be ruled out that the change in morphology is related to the presence of chloride ions. These results clearly indicate that soluble tin ions in the synthesis gel are responsible for the change in morphology.

### 3.3. Catalytic activity

As mentioned previously, almost all samples prepared in this study contained small amounts of $SnO_2$ particles on the surface of the Sn-Beta crystals. Tin oxide has previously been found to be inactive in the conversion of DHA to methyl lactate.[5]

To investigate the catalytic activity of the materials, the catalysts were tested in the conversion of 1,3-dihydroxyacetone (DHA) to methyl lactate (ML).[5] A very high substrate to catalyst ratio ($m_{DHA}/m_{catalyst}$ = 12) and a short reaction time was used (2 hours). The reaction conditions were intended to keep the conversion low in order to investigate the initial activity of the samples with varying tin content and crystallinity. Any contribution from leached tin species from the Sn-Beta zeolites under reaction conditions was found to be negligible (Figure S5).

Figure 9a shows the obtained ML yield for a sample with a Si/Sn ratio = 150 as a function of crystallization time. As the crystallinity increased from 20 to 63% (after 7 days), the ML yield remained below 5%. This is comparable to the yield of a blank experiment (3.7±0.1%). An onset in activity is observed after 10 days of crystallization (83% crystallinity) with an obtained yield of ML of 13.8±0.6% increasing after 14 days (>95% crystallinity) to 22±4%. The Sn-Beta catalyst is relatively inactive until late in the crystallization. Simple pore blocking by amorphous material in the partial crystalline samples could explain this observation.

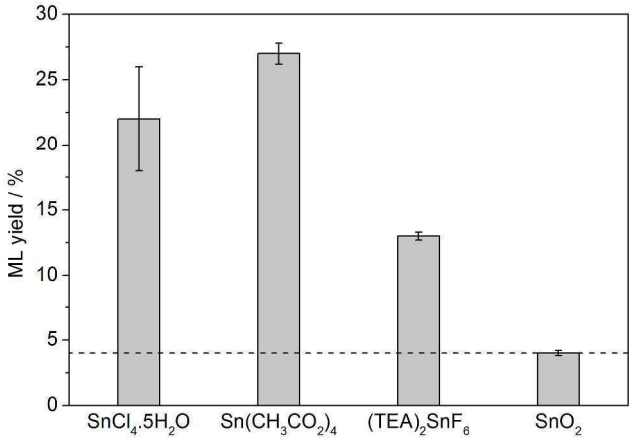


Figure 10. ML yield obtained with Sn-Beta prepared using different tin sources. The dashed line shows the yield when no catalyst is present. Reaction conditions: 25 mg catalyst, 300 mg DHA, 6.5 mL methanol, 600 rpm, 75°C, 2 hours.

Figure 9b shows the ML yield obtained from DHA in methanol with samples of varying tin content. It is evident that a large increase in ML yield coincides with the point of full crystallization (>95% crystallinity) of the series (see Table S1 for more information). A ML yield of 10.7±0.9% (4 days) was obtained for a Si/Sn ratio of 400 whereas for Si/Sn ratios of 200 and 100, ML yields of 23±3% (7 days) and 32±5% (60 days) were obtained, respectively. Although Sn-Beta is active with low tin content for this reaction, it is clear that the activity can be improved by incorporation of increasing amounts of tin. However, in all the cases the crystallinity needs to be above 80% to reach maximum activity. For two of the series (Si/Sn = 200 and Si/Sn = 400), a decrease in catalytic activity is observed for samples crystallized excessively longer than what is required to obtain a crystalline sample. For a Si/Sn ratio of 200, the obtained ML yield decreases from 27% (14 days) to 18% (30 days). The observation that the catalyst activity decreases for excessive synthesis times is very important when preparing the material for catalytic use. As explained in the previous section, Ostwald ripening phenomenon has been identified in the samples.

Finally, the catalytic activity was measured for samples prepared with other tin sources, see Figure 10. Sn-Beta samples prepared using tin(IV) acetate and $(TEA)_2SnF_6$ were both found to be active in the conversion of DHA to ML. However, only tin(IV) acetate (27% ML) gave comparable yields to tin(IV) chloride (22% ML) with $(TEA)_2SnF_6$ only giving a yield of 13% ML. When insoluble $SnO_2$ nanoparticles were used as a source of tin, the material was inactive (4% ML) comparable to the blank experiment (4% ML). These results illustrate that framework Sn sites are the active sites in the reaction and that the morphology changes are a consequence of the incorporation of tin in the framework.

## Conclusions

In this present study, we have shown that the addition of tin during near-neutral conditions in a fluoride medium severely retards the crystallization and changes the preferred growth of the crystal faces. A clear correlation was found between the tin content present during synthesis and the change in the capped square bipyramidal morphology. This was observed as a change from highly elongated crystals with low tin contents to highly truncated, almost plate-like, crystal at high tin contents.

Furthermore, tin was found to be unevenly distributed within the bulk of the crystal. Regardless of tin content and resulting morphology, a clear gradient in the distribution of tin within the bulk crystal was observed using SEM-WDS for all samples. The tin enriched shell was observed to extend roughly half the crystal radius and contain approximately twice the amount of tin as the depleted core. This feature was found to exist in samples even before being fully crystalline in appearance and was surprisingly found in crystals that continuously increased in size from Ostwald ripening. Tin was additionally found in small amounts present as nanosized tin oxide particles on the surface of the crystals.

The catalytic activity of the prepared Sn-Beta materials for the conversion of the triose sugar 1,3-dihydroxyacetone to methyl lactate was likewise found to depend on the tin content with increasing activity following increasing tin incorporation. The activity was found to not directly follow the crystallization of the materials. Instead any activity of the material appeared to be introduced in the very late stages of the crystal growth. Even though the physical properties such as degree of crystallinity, pore volume etc. were unchanged at prolonged synthesis times, we observed a decrease in the catalytic activity of the material as a function of prolonged synthesis time indicating that thorough control of the crystallization of Sn-Beta is required in order to make a good catalyst, also indicating that optimizing the catalyst could be done by reducing the crystal size. Furthermore, Sn-Beta was successfully prepared using a variety of tin sources including tin(IV) chloride, tin(IV) acetate and tetraethylammonium hexafluorostannate yielding active catalysts for the conversion of 1,3-dihydroxyacetone to methyl lactate and all having similar slightly truncated morphologies. When using tin(IV) oxide particles as the tin source no activity was obtained and the crystals resembled purely siliceous Beta crystals by being highly elongated with a distribution of $SnO_2$ particles on the surface of the crystals.

These findings point out that careful control of the synthesis parameters is required in order to optimize the catalytic activity of the Sn-Beta when prepared in a fluoride medium. In addition, direct turnover number comparisons for different Sn-Beta materials, based on the amount of tin in the samples is likely to give an over-simplified picture of the number of accessible active sites, as the tin gradient distribution, crystal morphology and Ostwald ripening will distort such an analysis, and a varying degree of active site accessibility may result for different samples.

## Acknowledgements

This work was supported by the Bio-Value platform (biovalue.dk), funded under the SPIR initiative by The Danish



 

Council for Strategic Research and The Danish Council for Technology and Innovation, case no: 0603-00522B.
D.D.F. and R.J.D gratefully acknowledge support from the National Science Foundation (Grant No. EEC-0813570).

## Notes and references

[a] Technical University of Denmark, Department of Chemistry, Kemitorvet, 2800-Kgs. Lyngby, Denmark.
[b] Haldor Topsøe A/S, New Business R&D, Nymøllevej 55, 2800-Kgs. Lyngby, Denmark e.
[c] University of Virginia, Department of Chemical Engineering, 102 Engineer's Way, PO Box 400741-Charlottesville, VA 22904, USA.
* Corresponding author. E-mail: esta@topsoe.dk Phone: +45 22754291.

† Electronic Supplementary Information (ESI) available: Further details are given in Tables S1-S2 and Figures S1-S5 as well as additional SE images and SEM-WDS measurements. See DOI: 10.1039/b000000x/

1. A. Corma, L. T. Nemeth, M. Renz and S. Valencia, *Nature*, 2001, **412**, 423-425.
2. A. Corma, M. E. Domine, L. Nemeth and S. Valencia, *J. Am. Chem. Soc.*, 2002, **124**, 3194-3195.
3. M. S. Holm, S. Saravanamurugan and E. Taarning, *Science*, 2010, **328**, 602-605.
4. M. Moliner, Y. Román-Leshkov and M. E. Davis, *Proc. Natl. Acad. Sci.*, 2010, **107**, 6164-6168.
5. E. Taarning, S. Saravanamurugan, H. M. Spangsberg, J. Xiong, R. M. West and C. H. Christensen, *ChemSusChem*, 2009, **2**, 625-627.
6. M. S. Holm, Y. J. Pagán-Torres, S. Saravanamurugan, A. Riisager, J. A. Dumesic and E. Taarning, *Green Chem.*, 2012, **14**, 702-706.
7. P. P. Pescarmona, K. P. F. Janssen, C. Delaet, C. Stroobants, K. Houthoofd, A. Philippaerts, C. De Jonghe, J. S. Paul, P. A. Jacobs and B. F. Sels, *Green Chem.*, 2010, **12**, 1083-1089.
8. E. T. H. Vink, K. R. Rábago, D. A. Glassner and P. R. Gruber, *Polym. Degrad. Stabil.*, 2003, **80**, 403-419.
9. J. Lunt, *Polym. Degrad. Stabil.*, 1998, **59**, 145-152.
10. J. Venus, *Biotechnol. J.*, 2006, **1**, 1428-1432.
11. R. Bermejo-Deval, R. S. Assary, E. Nikolla, M. Moliner, Y. Roman-Leshkov, S.-J. Hwang, A. Palsdottira, D. Silverman, R. F. Lobo, L. A. Curtiss and M. E. Davis, *Proc. Natl. Acad. Sci.*, 2012, **109**, 9727-9732.
12. M. Boronat, P. Concepcion, A. Corma, M. Renz and S. Valencia, *J. Catal.*, 2005, **234**, 111-118.
13. P. Wolf, M. Valla, A. J. Rossini, A. Comas-Vives, F. Núñez-Zarur, B. Malaman, A. Lesage, L. Emsley, C. Copéret and I. Hermans, *Angew. Chem., Int. Ed.*, 2014, **53**, 10179-10183.
14. C. M. Osmundsen, M. S. Holm, S. Dahl and E. Taarning, *Proc. R. Soc. A*, 2012, **468**, 2000-2016.
15. S. Roy, K. Bakhmutsky, E. Mahmoud, R. F. Lobo and R. J. Gorte, *ACS Catal.*, 2013, **3**, 573-580.
16. W. R. Gunther, V. K. Michaelis, M. A. Caporini, R. G. Griffin and Y. Roman-Leshkov, *J. Am. Chem. Soc.*, 2014, **136**, 6219-6222.
17. M. A. Camblor, A. Mifsud and J. Pérez-Pariente, *Zeolites*, 1991, **11**, 792-797.
18. J. Pérez-Pariente, J. A. Martens and P. A. Jacobs, *Appl. Catal.*, 1987, **31**, 35-64.
19. J. Pérez-Pariente, J. A. Martens and P. A. Jacobs, *Zeolites*, 1988, **8**, 46-53.
20. M. A. Camblor and J. Pérez-Pariente, *Zeolites*, 1991, **11**, 202-210.
21. M. J. Eapen, K. S. N. Reddy and V. P. Shiralkar, *Zeolites*, 1994, **14**, 295-302.
22. N. K. Mal and A. V. Ramaswamy, *Chem. Commun.*, 1997, 425-426.
23. J. Yu, in *Studies in Surface Science and Catalysis*, eds. J. Čejka, H. v. Bekkum, A. Corma and F. Schüth, Elsevier, 2007, pp. 39-103.
24. T. Blasco, M. A. Camblor, A. Corma, P. Esteve, J. M. Guil, A. Martinez, J. A. Perdigon-Melon and S. Valencia, *J. Phys. Chem. B*, 1998, **102**, 75-88.
25. M. A. Camblor, A. Corma and S. Valencia, *Chem. Commun.*, 1996, 2365-2366.
26. O. Larlus and V. Valtchev, *Microporous Mesoporous Mater.*, 2006, **93**, 55-61.
27. J. Cejka, A. Corma, S. Zones and Editors, *Zeolites And Catalysis: Synthesis, Reactions And Applications*, Wiley-VCH Verlag GmbH & Co. KGaA, 2010.
28. C.-C. Chang, Z. Wang, P. Dornath, H. Je Cho and W. Fan, *RSC Adv.*, 2012, **2**, 10475-10477.
29. Z. Kang, X. Zhang, H. Liu, J. Qiu and K. L. Yeung, *Chem. Eng. J.*, 2013, **218**, 425-432.
30. C. Hammond, S. Conrad and I. Hermans, *Angew. Chem., Int. Ed.*, 2012, **51**, 11736-11739.
31. P. Li, G. Liu, H. Wu, Y. Liu, J.-g. Jiang and P. Wu, *J. Phys. Chem. C*, 2011, **115**, 3663-3670.
32. J. Dijkmans, D. Gabriels, M. Dusselier, F. de Clippel, P. Vanelderen, K. Houthoofd, A. Malfliet, Y. Pontikes and B. F. Sels, *Green Chem.*, 2013, **15**, 2777-2785.
33. S. Valencia and A. Corma, UOP LLC, 1999.
34. N. V. Y. Scarlett and I. C. Madsen, *Powder Diffr.*, 2006, **21**, 278-284.
35. O. Larlus and V. P. Valtchev, *Chem. Mater.*, 2005, **17**, 881-886.
36. D. P. Serrano, R. Van Grieken, P. Sánchez, R. Sanz and L. Rodríguez, *Microporous and Mesoporous Mater.*, 2001, **46**, 35-46.
37. U. Schubert and N. Hüsing, *Synthesis of Inorganic Materials*, Wiley-VCH, Weinheim, 2005.
38. P. W. Voorhees, *J. Stat. Phys.*, 1985, **38**, 231-252.
39. J. Sun, G. Zhu, Y. Chen, J. Li, L. Wang, Y. Peng, H. Li and S. Qiu, *Microporous and Mesoporous Mater.*, 2007, **102**, 242-248.
40. D. G. Hay, H. Jaeger and K. G. Wilshier, *Zeolites*, 1990, **10**, 571-576.
41. C. S. Cundy and P. A. Cox, *Microporous and Mesoporous Mater.*, 2005, **82**, 1-78.
42. Y. Chen, G. Zhu, Y. Peng, X. Yao and S. Qiu, *Microporous and Mesoporous Mater.*, 2009, **124**, 8-14.

During synthesis of Sn-Beta, tin affects the crystallization rate, morphology and is incorporated in an outer shell of the crystal.